PRIN 2017 Final workshop – Innovative numerical methods for evolutionary partial differential equations and applications
Dedicated to the memory of Maurizio Falcone
20-22 February 2023 – Catania, Italy

Numerical treatment of boundary conditions for blood flow modeling in networks of viscoelastic vessels

Francesco Piccioli[†], Giulia Bertaglia[*], Alessandro Valiani[†], and **Valerio Caleffi**[†]

[†] Department of Engineering, University of Ferrara
[*]Department of Environmental and Prevention Sciences, University of Ferrara

University of Ferrara

Context

- The numerical modelling of blood flow in cardiovascular networks provide satisfactory results only if the mechanical behavior of vessels is correctly accounted for[1]. In particular, an accurate viscoelastic characterization of the vessel wall is crucial.
- In previous works, we have proposed a Standard Linear Solid model (SLSM) to describe the vessel wall rheology[2,3], enabling to simulate the most significant aspects related to the viscoelasticity of the vessel wall: the exponential decay in time of the stress and the creep phenomena. This allows to account for damping effects related to the partial dissipation of energy.

Motivation

- Although the viscoelasticity is usually neglected in the implementation of internal and external boundary conditions, in favor of a local elastic approach, we believe that the inclusion of the viscoelastic contribution at boundaries is mandatory for a correct hemodynamic analysis[4].
- This work presents a methodology for modelling cardiovascular networks accounting for the viscoelastic behavior of blood vessels also in the treatment of the inflow/outflow boundaries and at the junctions.

[1] L. Formaggia, D. Lamponi, and A. Quarteroni (2003), *J. Eng. Math.* 47.
[2] G. Bertaglia, V. Caleffi, and A. Valiani (2020), *Comput. Methods Appl. Mech. Eng.* 360.
[3] G. Bertaglia, A. Navas-Montilla, A. Valiani, M. I. Monge Garcìa, J. Murillo, and V. Caleffi (2020), *J. Biomech.* 100.
[4] L.O. Muller, G. Leugering, and P.J. Blanco (2016), *J. Comput. Phys.* 314.

Mathematical model

The mathematical model for the blood flow in the single vessel is the *augmented fluid-structure interaction* (a-FSI) *system*[2]:

$$\begin{cases} \partial_t A + \partial_x(Au) = 0 \\ \partial_t(Au) + \partial_x(Au^2) + \dfrac{A}{\rho}\partial_x p = \dfrac{f}{\rho} \\ \partial_t p + d\,\partial_x(Au) = S \\ \partial_t A_0 = 0 \\ \partial_t E_0 = 0 \\ \partial_t p_{ext} = 0 \end{cases}$$

Eq. continuity

Eq. momentum

Viscoelastic tube law

Closing equations for longitudinal discontinuities

$$\partial_t \boldsymbol{Q} + \partial_x \boldsymbol{f}(\boldsymbol{Q}) + \boldsymbol{B}(\boldsymbol{Q})\,\partial_x \boldsymbol{Q} = \boldsymbol{S}(\boldsymbol{Q}) \quad \text{or} \quad \partial_t \boldsymbol{Q} + \boldsymbol{A}(\boldsymbol{Q})\,\partial_x \boldsymbol{Q} = \boldsymbol{S}(\boldsymbol{Q})$$

[2] G. Bertaglia, VC, and A. Valiani (2020), *Comput. Methods Appl. Mech. Eng.* 360.

Viscoelastic tube law

The SLSM model is defined by three parameters:

- The instantaneous Young modulus, $\boldsymbol{E_0(x)}$;
- The asymptotic Young modulus, $\boldsymbol{E_\infty(x)}$;
- The relaxation time, $\boldsymbol{\tau_r(x)}$.

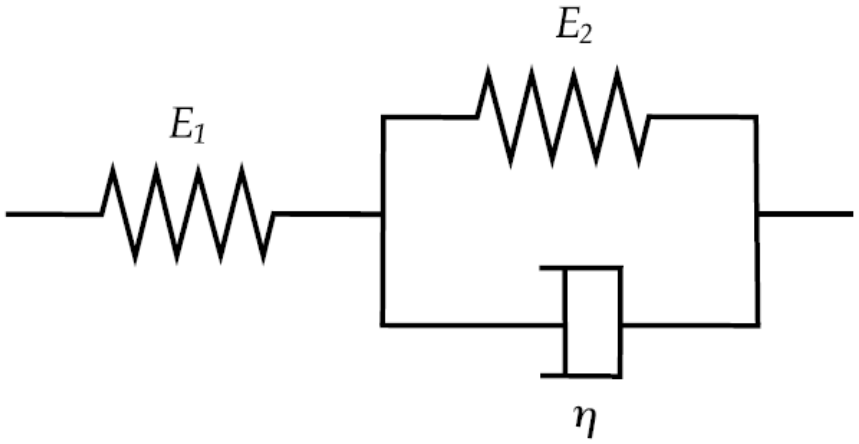

The instantaneous behaviour is governed by three parameters ***K***, ***m*** and ***n***.

$$\partial_t p + \underbrace{\left[\frac{K}{A}\left(m\,\alpha^m - n\,\alpha^n\right)\right]}_{d}\partial_x(Au) = \underbrace{\frac{1}{\tau_r}\left[\frac{E_\infty}{E_0}K(\alpha^m - \alpha^n) - (p - p_{ext})\right]}_{S}$$

Riemann Invariants

In the physiological range of the parameters, the a-FSI *system* is (*not strictly*) hyperbolic and can be written in quasi-linear form and is characterized by:

- 4 linearly degenerated fields, associated with contact discontinuity waves and Riemann Invariants:

$$\Gamma_1^{LD} = Au, \qquad \Gamma_2^{LD} = p + \frac{1}{2}\rho u^2$$

- 2 genuinely non-linear fields, associated with either shocks or rarefactions and Riemann Invariants:

$$\Gamma_{1,2} = u \pm \int \frac{c(A)}{A}\,\mathrm{d}A\,, \qquad \boxed{\Gamma_3 = p - \int d(A)\mathrm{d}A}$$

Numerical scheme

Space discretization **Finite Volume (FV) method** – TVD estrapolation – **minmod limiter**

$$\Delta \boldsymbol{Q}_i^{(k)} = \text{minmod}\left(\boldsymbol{Q}_i^{(k)} - \boldsymbol{Q}_{i-1}^{(k)}, \boldsymbol{Q}_{i+1}^{(k)} - \boldsymbol{Q}_i^{(k)}\right) \qquad \boldsymbol{Q}_{i\pm\frac{1}{2}}^{(k),\mp} = \boldsymbol{Q}_i^{(k)} \pm \Delta \boldsymbol{Q}_i^{(k)}$$

Time discretization A stiffly accurate **IMEX-SSP(3,3,2)** scheme is used. The scheme is asymptotic preserving (AP) and asymptotic accurate in the zero relaxation limit[2,5,6].

- An **L-stable diagonally implicit Runge-Kutta** scheme is used for the *stiff part*
- An **explicit SSP** scheme is provided for *non-stiff part*

$$\boldsymbol{Q}_i^{(k)} = \boldsymbol{Q}_i^n - \frac{\Delta t}{\Delta x}\sum_{j=1}^{k-1} \tilde{a}_{kj}\left[\left(\boldsymbol{F}_{i+\frac{1}{2}}^{(j)} - \boldsymbol{F}_{i-\frac{1}{2}}^{(j)}\right) + \left(\boldsymbol{D}_{i+\frac{1}{2}}^{(j)} - \boldsymbol{D}_{i-\frac{1}{2}}^{(j)}\right) + \boldsymbol{B}\left(\boldsymbol{Q}_i^{(j)}\right)\Delta \boldsymbol{Q}_i^{(j)}\right] + \Delta t \sum_{j=1}^{k} a_{kj}\boldsymbol{S}\left(\boldsymbol{Q}_i^{(j)}\right)$$

$$\boldsymbol{Q}_i^{n+1} = \boldsymbol{Q}_i^n - \frac{\Delta t}{\Delta x}\sum_{k=1}^{s} \tilde{\omega}_k\left[\left(\boldsymbol{F}_{i+\frac{1}{2}}^{(k)} - \boldsymbol{F}_{i-\frac{1}{2}}^{(k)}\right) + \left(\boldsymbol{D}_{i+\frac{1}{2}}^{(k)} - \boldsymbol{D}_{i-\frac{1}{2}}^{(k)}\right) + \boldsymbol{B}\left(\boldsymbol{Q}_i^{(k)}\right)\Delta \boldsymbol{Q}_i^{(k)}\right] + \Delta t \sum_{k=1}^{s} \omega_k\boldsymbol{S}\left(\boldsymbol{Q}_i^{(k)}\right)$$

Numerical fluxes and non conservative jumps are obtained applying the DOT solver[7]

[2] G. Bertaglia, VC, and A. Valiani (2020), *Comput. Meth. Appl. Mech. Eng.* 360.
[5] G. Bertaglia, VC, L. Pareschi, and A. Valiani (2021), *J. Comput. Phys.* 430.
[6] L. Pareschi, and G. Russo (2005), *J. Sci. Comput.* 25.
[7] M. Dumbser, E.F. Toro, (2011), *J. Sci. Comput.* 48.

Numerical scheme

$\boldsymbol{F}$ and $\boldsymbol{D}$ are the vectors of numerical fluxes and non-conservative jumps, evaluated at the cell boundaries though the path-conservative Dumbser-Osher-Toro (DOT) Riemann solver [7].

$$\boldsymbol{F}_{i\pm\frac{1}{2}} = \frac{1}{2}\left[\boldsymbol{f}\left(\boldsymbol{Q}^{+}_{i\pm\frac{1}{2}}\right) + \boldsymbol{f}\left(\boldsymbol{Q}^{-}_{i\pm\frac{1}{2}}\right)\right] - \frac{1}{2}\int_0^1 \left|\boldsymbol{A}\left(\Psi\left(\boldsymbol{Q}^{-}_{i\pm\frac{1}{2}}, \boldsymbol{Q}^{+}_{i\pm\frac{1}{2}}, s\right)\right)\right| \frac{\partial \Psi}{\partial s}\,\mathrm{d}s$$

$$\boldsymbol{D}_{i\pm\frac{1}{2}} = \frac{1}{2}\int_0^1 \left|\boldsymbol{B}\left(\Psi\left(\boldsymbol{Q}^{-}_{i\pm\frac{1}{2}}, \boldsymbol{Q}^{+}_{i\pm\frac{1}{2}}, s\right)\right)\right| \frac{\partial \Psi}{\partial s}\,\mathrm{d}s$$

[7] M. Dumbser, E.F. Toro, (2011), *J. Sci. Comput.* 48.

Boundaries of the network

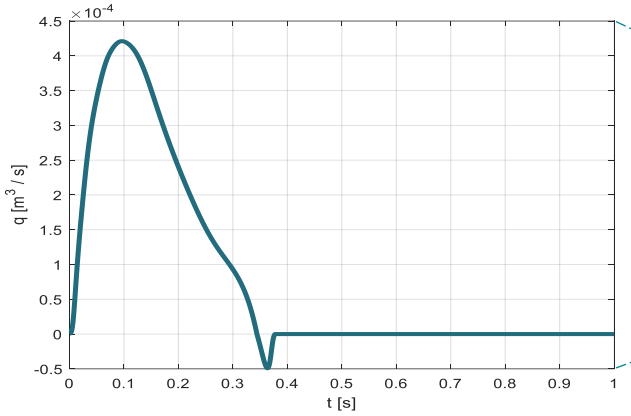

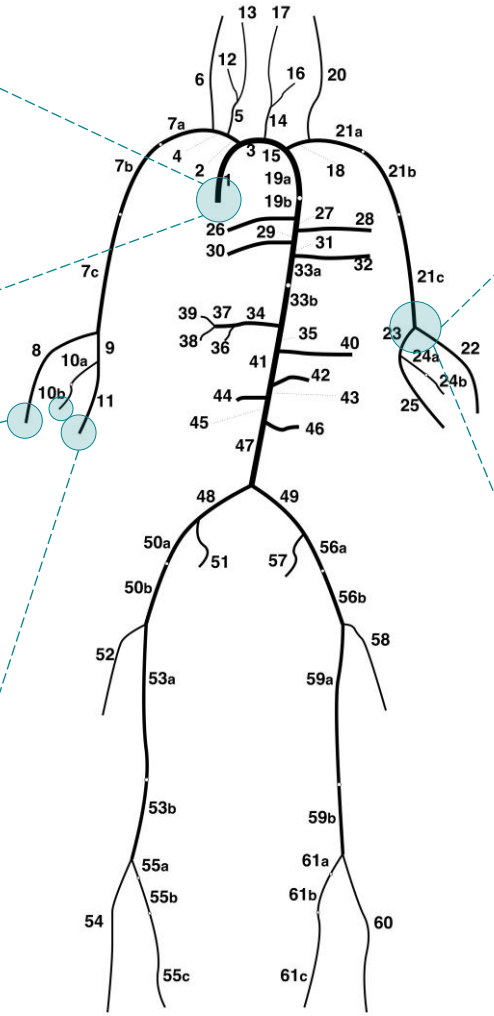

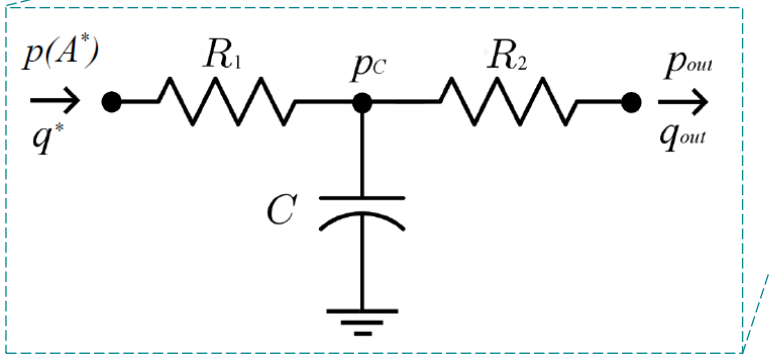

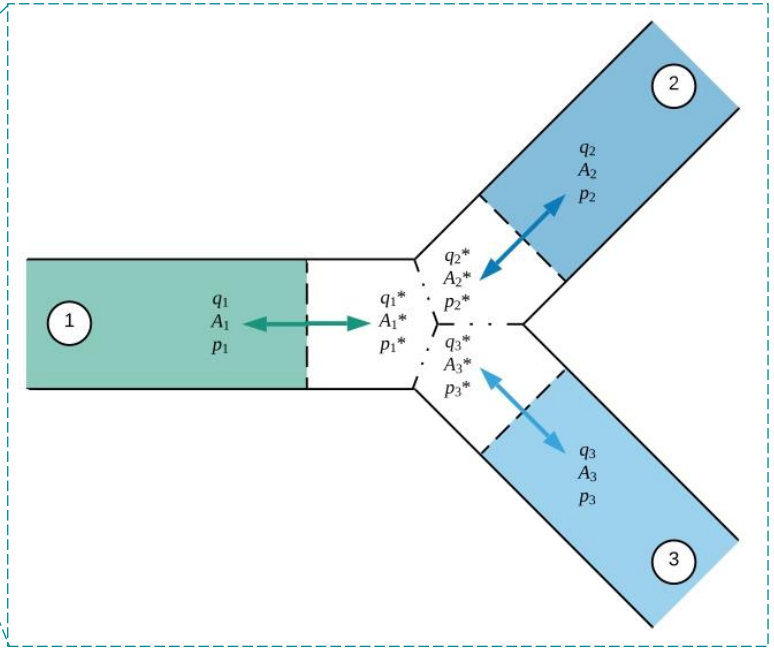

Boundary conditions

Venous return

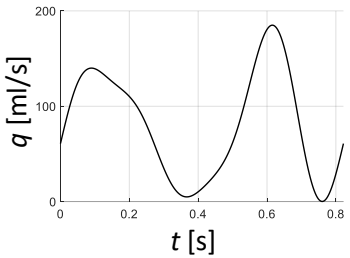

Left atrium

Mitral valve

Left ventricle

Aortic valve

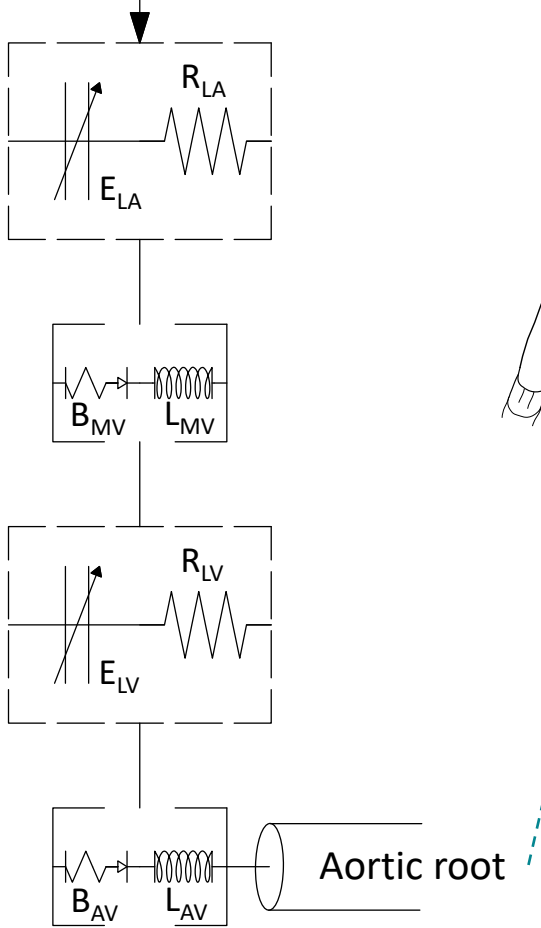

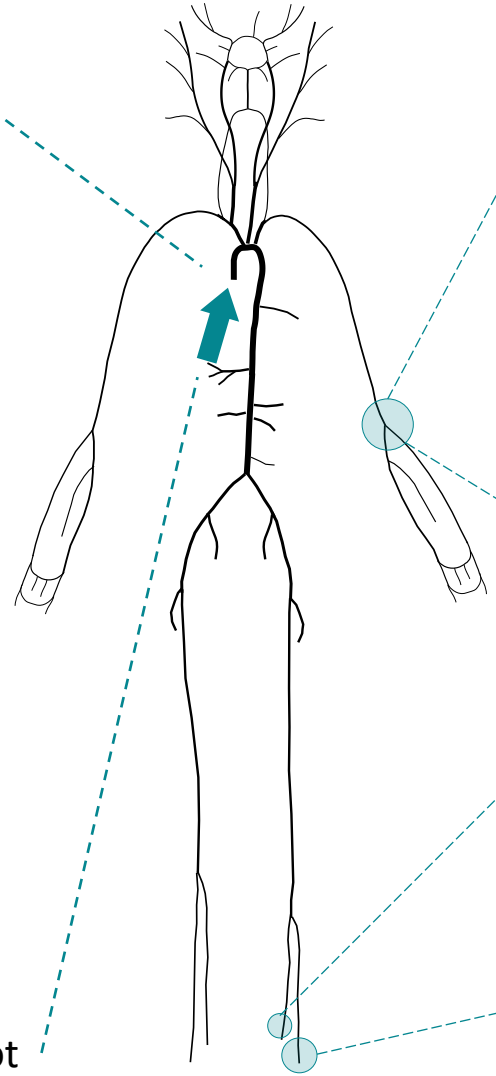

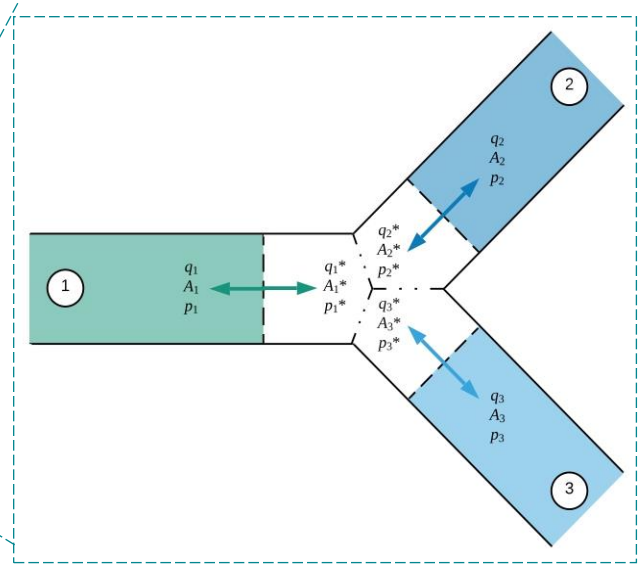

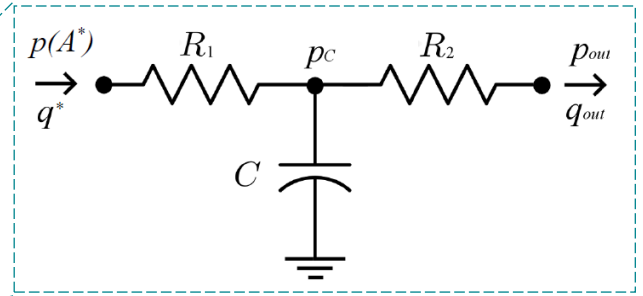

Cardiac contraction model

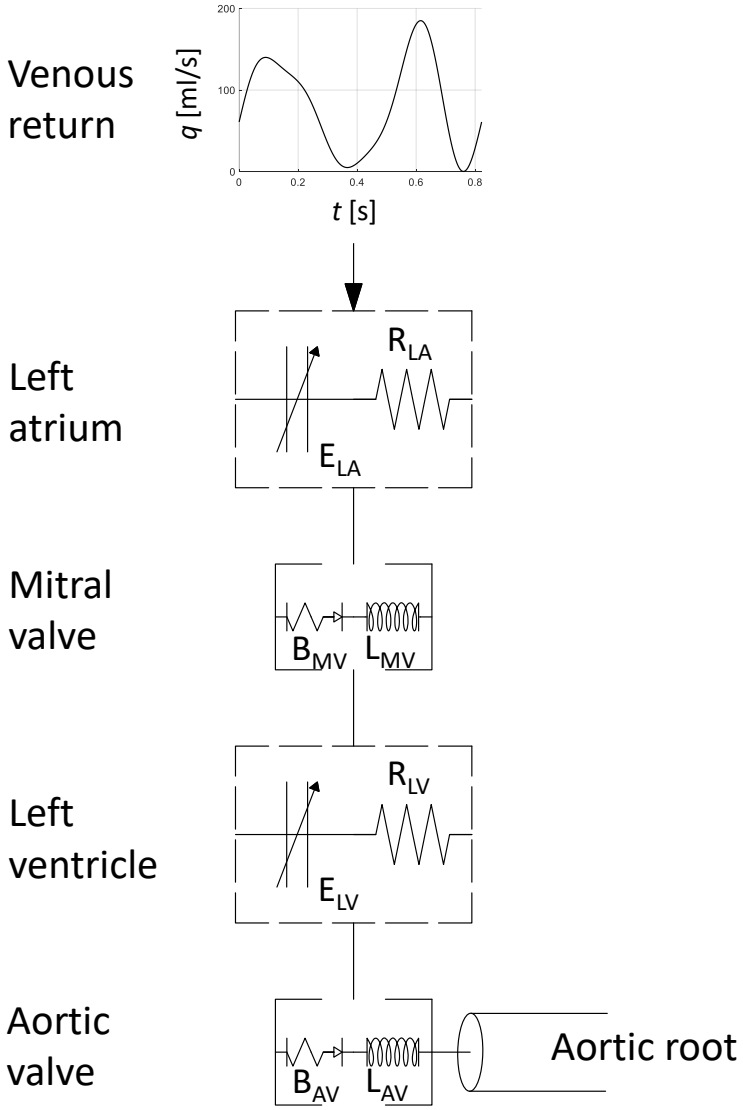

$$E(t) = \left[\frac{E_{max} - E_{min}}{\max\left(H_1(t)H_2(t)\right)}\right] H_1(t)H_2(t) + \mathrm{E}_{min}$$

$$p(t) = E(t)\left[v(t) - v_{p0}\right] - Rq_{out}(\mathrm{t})$$

$$\frac{\mathrm{d}v}{\mathrm{d}t} = q_{in}(t) - q_{out}(t)$$

$$\frac{\mathrm{d}\zeta}{\mathrm{d}t} = \mathcal{F}(\zeta, K_{vo}, K_{vc}, \Delta p) = \begin{cases} [1 - \zeta(t)]K_{vo}\Delta p(t) & \text{if } \Delta p(t) > 0 \\ \zeta(t)K_{vc}\Delta p(t) & \text{if } \Delta p(t) < 0 \end{cases}$$

$$\frac{\mathrm{d}q}{\mathrm{d}t} = \frac{1}{L(t)}\left[\Delta p(t) - B(t)q(t)|q(t)|\right]$$

Cardiac contraction model

Equations that govern the cardiac contraction model are integrated in time following the IMEX-RK scheme, treating the equations explicitly since they do not contain any *stiff* term.

$$q_v^{(k)} = q_v^n + \Delta t \sum_{j=1}^{k-1} \tilde{a}_{kj} \left[\frac{1}{L^{(j)}} \left(\Delta p^{(j)} - B^{(j)} q^{(j)} \left| q^{(j)} \right| \right) \right]$$

$$q_v^{n+1} = q_v^n + \Delta t \sum_{k=1}^{s} \tilde{\omega}_k \left[\frac{1}{L^{(k)}} \left(\Delta p^{(k)} - B^{(k)} q^{(k)} \left| q^{(k)} \right| \right) \right]$$

$\zeta(t)$ and $v(t)$ are integrated following the same approach.

Junctions

The numerical modelling of the internal boundaries is derived from the solution of an extended Riemann problem (RP), here called the Junction Riemann problem (JRP).

We remember that for a classic 1D RP :

- the RP – involving only a continuity equation and a momentum equation – is characterised by a solution constituted by one intermediate constant state (the star region) separated from the initially imposed constant states by non-linear waves (shock waves or rarefactions).
- Adding a further equations to account for mechanical discontinuities results in an enrichment of the eigenstructure with null eigenvalues and stationary contact waves become part of the solution.
- restricting the analysis to sub-critical flows, the non-linear waves are directed from the centre to the periphery, the intermediate constant state become two, separated from each other by a new stationary contact discontinuity wave.

Junctions

The extension to the JRP follows:

- Conceiving the position of the initial discontinuity as a junction section among branches, the RP partial solution related to each branch consists of an initial state separated from the star region of the same branch by a non-linear wave, while the intermediate states of the branching vessels, adjacent to the node, are separated from each other by contact discontinuities.

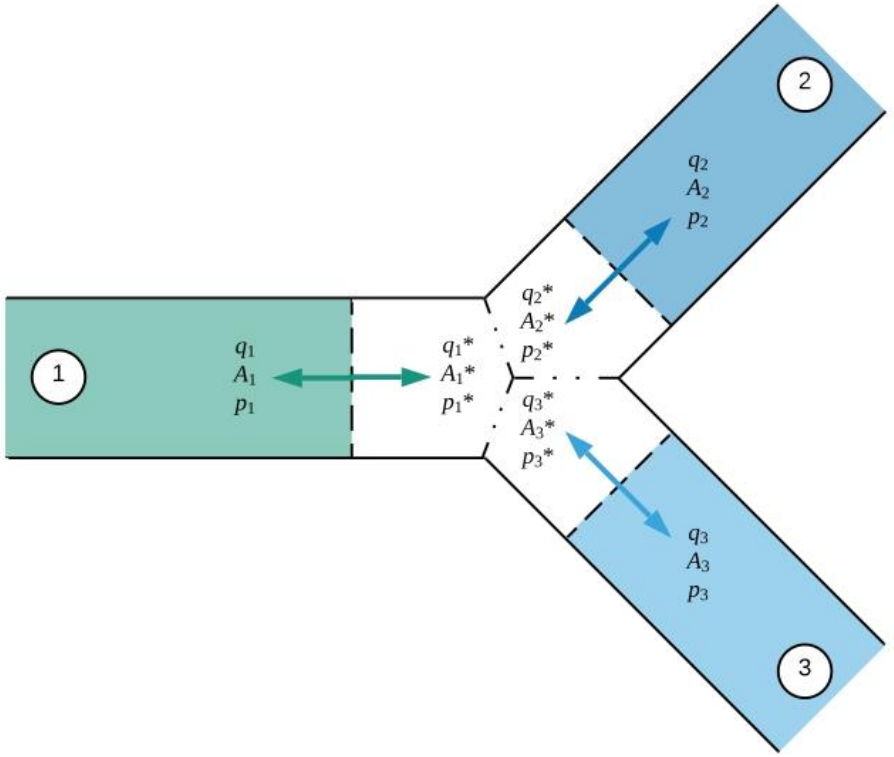

Junctions

The unknowns of the JRP are the flow rate, q_j^*, the cross-sectional area, A_j^*, and pressure, p_j^*, of the star region for each branching vessel.

$$\begin{cases} \sum_{i=1}^{N} \Theta_{n_i} A_i^* u_i^* = 0 \\ \left(p_1^* + \frac{1}{2}\rho {u_1^*}^2\right) - \left(p_i^* + \frac{1}{2}\rho {u_i^*}^2\right) = 0 \quad i = 2, \dots, N \\ u_i^* - u_i^{1D} + \Theta_{n_i} \int_{A_i^{1D}}^{A_i^*} \frac{c(A)}{A} \mathrm{d}A = 0 \quad i = 1, \dots, N \\ p_i^* - p_i^{1D} + \int_{A_i^{1D}}^{A_i^*} d(A) \mathrm{d}A = 0 \quad i = 1, \dots, N \end{cases}$$

Mass

Total pressure

Second order accuracy at boundaries

At boundaries, the solution obtained from the computation of the boundary condition (i.e., JRP, inlet, outlets) is used to compensate for the missing cell average values in the slope computation:

$$\Delta \boldsymbol{Q}_1^{(k)} = \text{minmod}(\mathbf{Q}_1^{(k)} - \mathbf{Q}_{BC}^{(k)}, \mathbf{Q}_2^{(k)} - \mathbf{Q}_1^{(k)})$$

$$\Delta \boldsymbol{Q}_{n_c}^{(k)} = \text{minmod}(\mathbf{Q}_{n_c}^{(k)} - \mathbf{Q}_{n_c-1}^{(k)}, \mathbf{Q}_{BC}^{(k)} - \mathbf{Q}_{n_c}^{(k)})$$

Validation tests

2-vessel artery

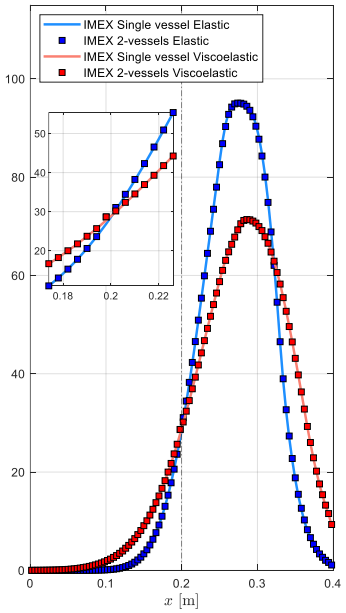

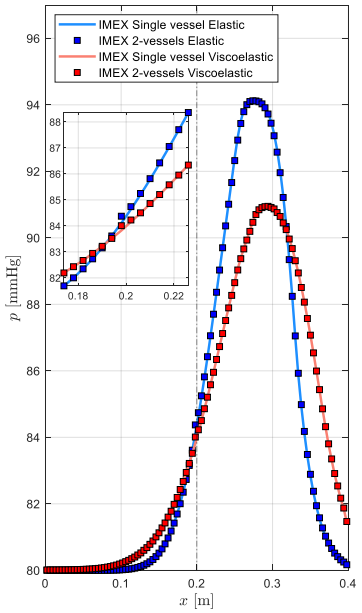

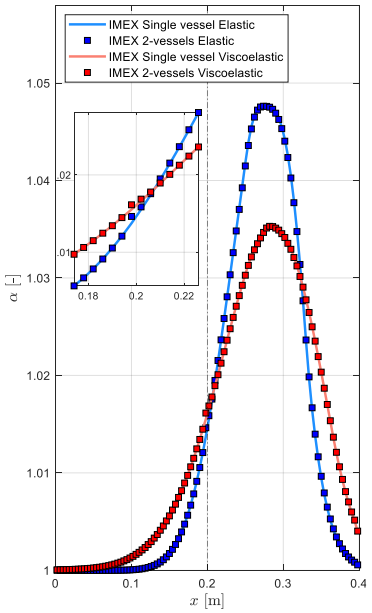

2-vessel vein

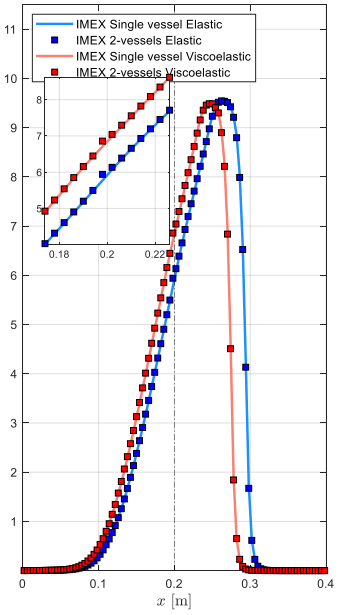

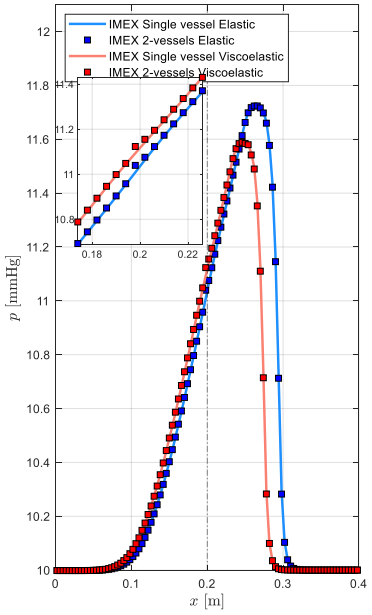

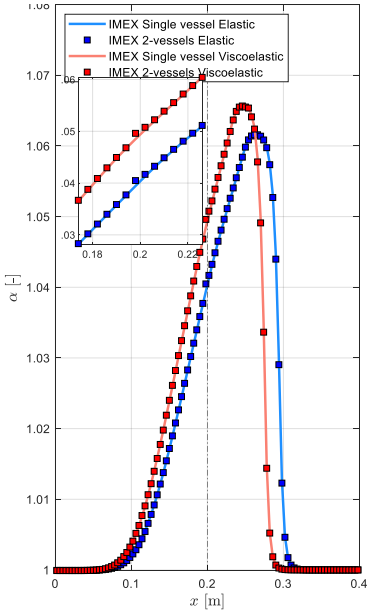

Test	Variable	n_c	L^1	$\mathcal{O}(L^1)$	L^2	$\mathcal{O}(L^2)$	L^∞	$\mathcal{O}(L^\infty)$
AA	A	33	3.47×10^{-8}	-	6.03×10^{-8}	-	1.36×10^{-7}	-
		99	3.75×10^{-9}	2.02	6.58×10^{-9}	2.02	1.48×10^{-8}	2.02
		297	4.13×10^{-10}	2.01	7.25×10^{-10}	2.01	1.64×10^{-9}	2.00
		891	4.52×10^{-11}	2.01	7.95×10^{-11}	2.01	1.80×10^{-10}	2.01
		2673	4.52×10^{-12}	2.10	7.94×10^{-12}	2.10	1.80×10^{-11}	2.10
	Au	33	1.70×10^{-7}	-	2.98×10^{-7}	-	7.51×10^{-7}	-
		99	2.38×10^{-8}	1.79	4.29×10^{-8}	1.77	1.16×10^{-7}	1.70
		297	2.82×10^{-9}	1.95	5.10×10^{-9}	1.94	1.40×10^{-8}	1.92
		891	3.16×10^{-10}	2.00	5.74×10^{-10}	2.00	1.58×10^{-9}	2.00
		2673	3.18×10^{-11}	2.10	5.78×10^{-11}	2.10	1.60×10^{-10}	2.10
	p	33	8.21	-	1.43×10^{1}	-	3.42×10^{1}	-
		99	9.14×10^{-1}	2.00	1.60	2.00	3.75	2.01
		297	1.00×10^{-1}	2.01	1.76×10^{-1}	2.01	4.12×10^{-1}	2.01
		891	1.10×10^{-2}	2.01	1.93×10^{-2}	2.01	4.52×10^{-2}	2.01
		2673	1.10×10^{-3}	2.10	1.93×10^{-3}	2.10	4.51×10^{-3}	2.10
VV	A	33	2.91×10^{-8}	-	9.49×10^{-8}	-	7.55×10^{-7}	-
		99	3.26×10^{-9}	2.00	1.11×10^{-8}	1.96	1.15×10^{-7}	1.71
		297	3.57×10^{-10}	2.01	1.21×10^{-9}	2.01	1.38×10^{-8}	1.93
		891	3.88×10^{-11}	2.02	1.34×10^{-10}	2.01	1.54×10^{-9}	2.00
		2673	3.87×10^{-12}	2.10	1.34×10^{-11}	2.10	1.55×10^{-10}	2.09
	Au	33	1.61×10^{-8}	-	7.34×10^{-8}	-	6.33×10^{-7}	-
		99	2.15×10^{-9}	1.83	9.46×10^{-9}	1.86	1.02×10^{-7}	1.59
		297	2.59×10^{-10}	1.93	1.15×10^{-9}	1.91	1.35×10^{-8}	1.91
		891	2.94×10^{-11}	1.99	1.32×10^{-10}	1.97	1.58×10^{-9}	1.95
		2673	2.97×10^{-12}	2.10	1.34×10^{-11}	2.10	1.61×10^{-10}	2.08
	p	33	6.55×10^{-1}	-	2.12	-	1.69×10^{1}	-
		99	8.89×10^{-2}	1.82	3.25×10^{-1}	1.71	3.54	1.42
		297	1.19×10^{-2}	1.83	4.77×10^{-2}	1.75	5.20×10^{-1}	1.75
		891	1.33×10^{-3}	2.00	5.44×10^{-3}	1.98	6.15×10^{-2}	1.94
		2673	1.37×10^{-4}	2.07	5.69×10^{-4}	2.05	6.48×10^{-3}	2.05

ADAN56 [4,5]

Aortic arch

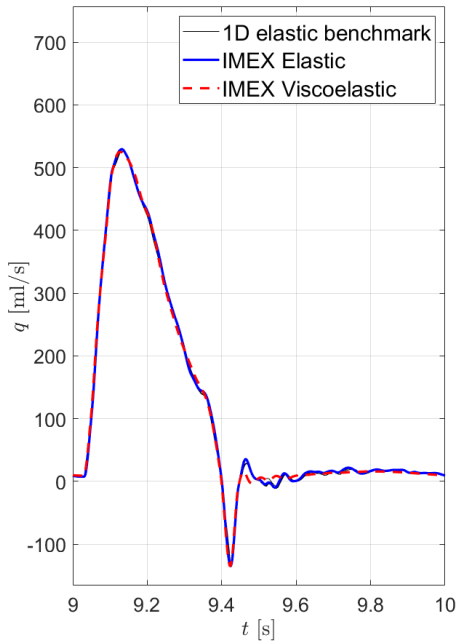

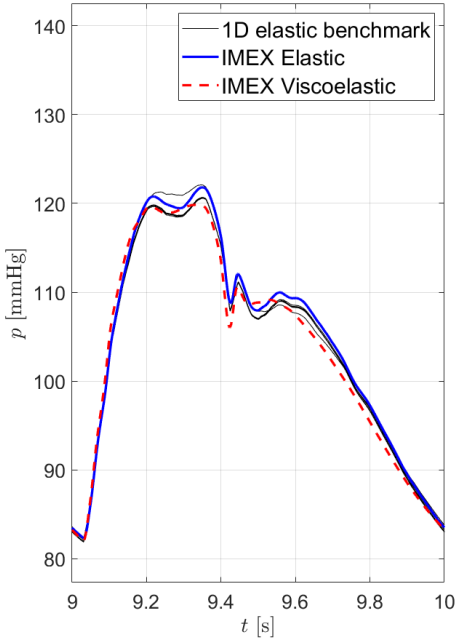

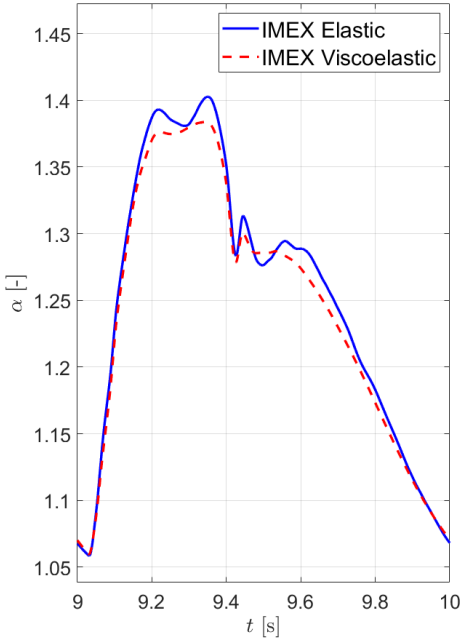

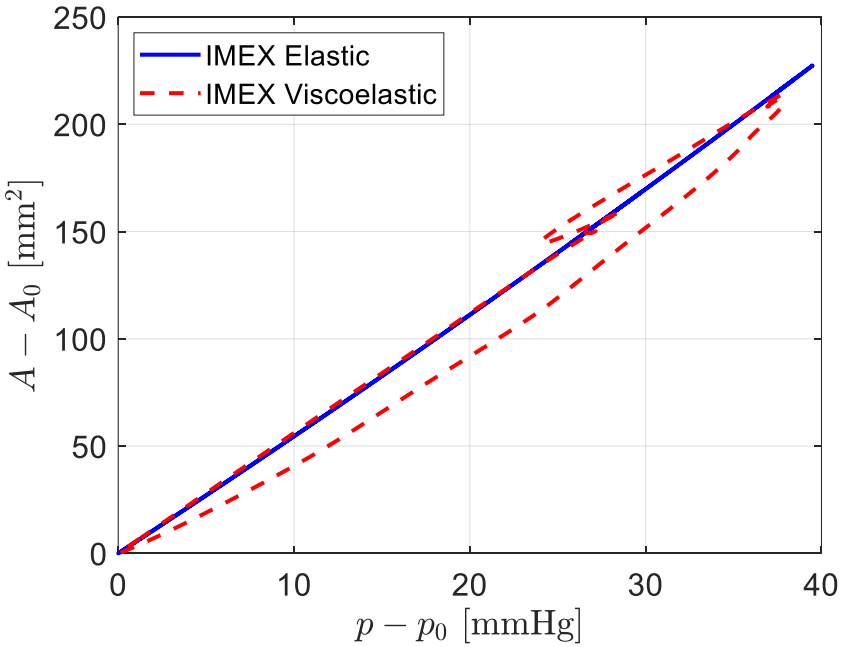

[4] P.J. Blanco et al. (2014, 2015)
[5] E. Boileau et al. (2015)

ADAN56

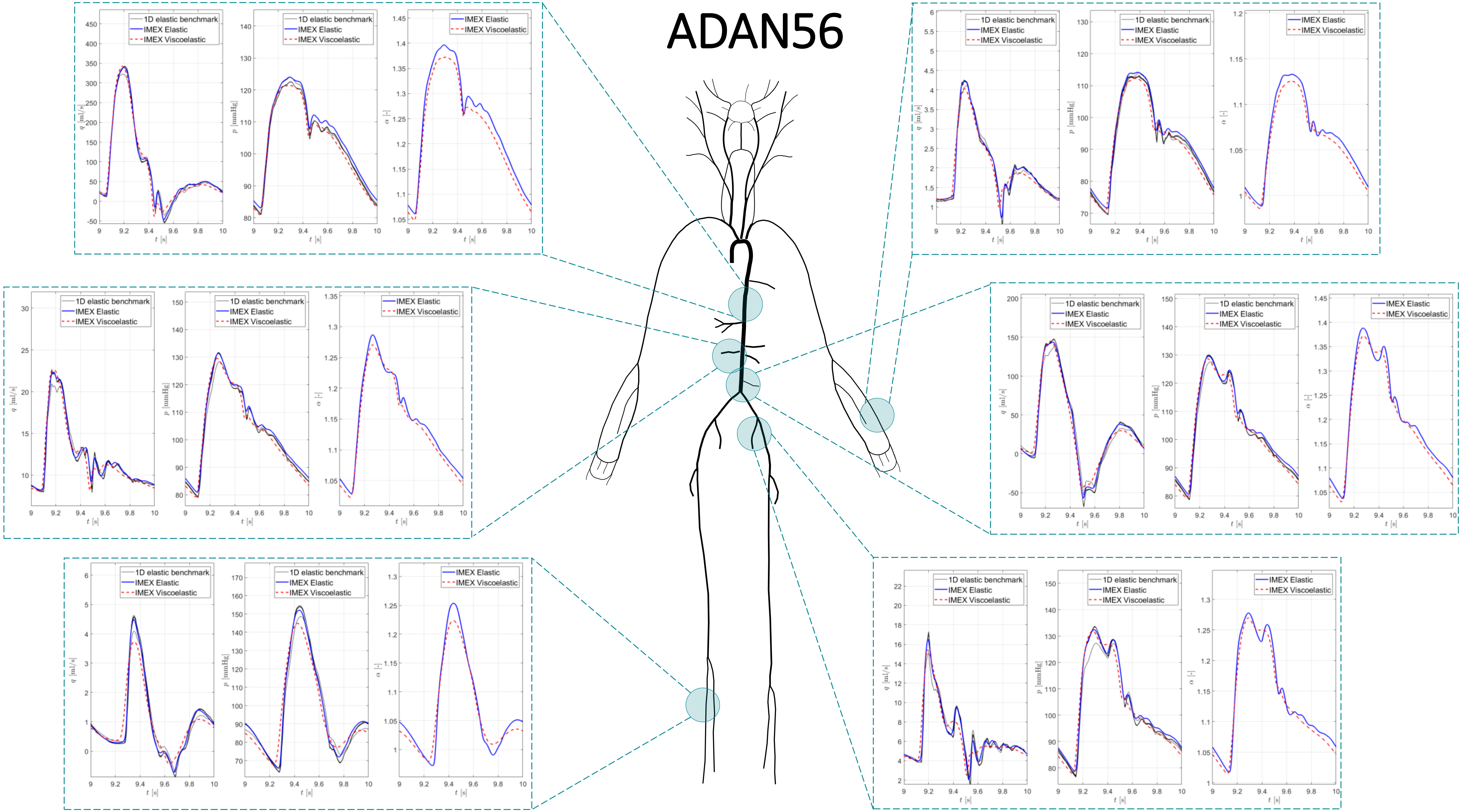
1D elastic benchmark
IMEX Elastic
IMEX Viscoelastic
q [ml/s]
p [mmHg]
α [-]
t [s]

Conclusions

Reference papers:

1. Modeling blood flow in viscoelastic vessels: the 1D augmented fluid–structure interaction system. G. Bertaglia, V. Caleffi, A. Valiani. Computer Methods in Applied Mechanics and Engineering, 360:112772, 2020.
2. Modeling blood flow in networks of viscoelastic vessels with the 1-D augmented fluid–structure interaction system, F. Piccioli, G. Bertaglia, A. Valiani, V. Caleffi, Journal of Computational Physics, 2022, Vol. 464, art. no. 111364.

Conclusions

1. Computational hemodynamics in arteries with the one-dimensional augmented fluid-structure interaction system: viscoelastic parameters estimation and comparison with in-vivo data. Bertaglia, G., Navas-Montilla, A., Valiani, A., Monge García, M. I., Murillo, J., & Caleffi, V. *Journal of Biomechanics*, 100, 109595, 2020.
2. Uncertainty quantification of viscoelastic parameters in arterial haemodynamics with the a-FSI blood flow model. Bertaglia G., Caleffi V., Pareschi L., Valiani A. *Jornal of Computational Physics*, 430: 110102, 2021.
3. The effect of cardiac properties on arterial pulse waves: An in-silico study. Piccioli F., Valiani A., Alastruey J., Caleffi V., *International Journal for Numerical Methods in Biomedical Engineering*, 1–27, 2022.

Thank you for your attention.

University of Ferrara

University of Ferrara